Observation of Double Impurity Critical Gradients for Electromagnetic Turbulence Excitation in Tokamak Plasmas

W. L. Zhong,[1,*] Y. Shen,[1] X. L. Zou,[2] J. M. Gao,[1] Z. B. Shi,[1] J. Q. Dong,[1,3] X. R. Duan,[1] M. Xu,[1] Z. Y. Cui,[1] Y. G. Li,[1] X. Q. Ji,[1] D. L. Yu,[1] J. Cheng,[1] G. L. Xiao,[1] M. Jiang,[1] Z. C. Yang,[1] B. Y. Zhang,[1] P. W. Shi,[1] Z. T. Liu,[1] X. M. Song,[1] X. T. Ding,[1] and Yong Liu[1]

(HL-2A Team)[1]

[1]*Southwestern Institute of Physics, P.O. Box 432, Chengdu 610041, People's Republic of China*
[2]*CEA, IRFM, F-13108 Saint-Paul-lez-Durance, France*
[3]*Institute for Fusion Theory and Simulation, Zhejiang University, Hangzhou 310027, People's Republic of China*
(Received 22 January 2016; revised manuscript received 13 June 2016; published 22 July 2016)

The impact of impurity ions on a pedestal has been investigated in the HL-2A Tokamak, at the Southwestern Institute of Physics, Chengdu, China. Experimental results have clearly shown that during the *H*-mode phase, an electromagnetic turbulence was excited in the edge plasma region, where the impurity ions exhibited a peaked profile. It has been found that double impurity critical gradients are responsible for triggering the turbulence. Strong stiffness of the impurity profile has been observed during cyclic transitions between the *I*-phase and *H*-mode regime. The results suggest that the underlying physics of the self-regulated edge impurity profile offers the possibility for an active control of the pedestal dynamics via pedestal turbulence.

DOI: 10.1103/PhysRevLett.117.045001

In toroidal fusion devices, such as tokamaks and stellarators, the edge plasma region often spontaneously forms a so-called pedestal with steep density and temperature gradients when the heating power is sufficiently high [1,2], and the high pressure gradient will drive the edge-localized modes (ELMs) which are magnetohydrodynamic (MHD) instabilities [3,4]. The improvement of the plasma confinement (termed as the *H mode*) is the result of the suppression of edge turbulence and the reduction of outward energy and particle transport in the pedestal region. Previous studies have shown that the divertor heat load in a burning plasma device may exceed several times the tolerable plasma facing material limits (10 $\mathrm{MW/m^2}$) [5]. One of the envisaged solutions is using impurity seeding for forming a steady-state edge radiation layer. It acts as an active control technique to lower the heat loads through converting the heat power flux into impurity seed radiation, and to minimize the impact of impurity radiation on the core confinement [6].

Furthermore, it has been found that the impurity seeding is a benefit for ELM control by affecting the pedestal dynamics and instabilities [7,8]. However, the role of impurities herein is hitherto unrecognized [8,9]. Especially, the effects of the impurity ions on pedestal turbulence and the underlying mechanisms have not been experimentally identified so far: It is needed to distinguish the excitation threshold of the turbulence. The turbulent transport thresholds have been intensively studied by experiments and theoretical simulations in plasma heat and particle transport [10–13]. It was found that the density and/or temperature critical gradients are responsible for the onset of turbulence and the profile stiffness. For tokamak plasmas, the plasma turbulence exhibits an electromagnetic feature as the plasma β (the ratio of plasma pressure p to magnetic pressure $B^2/2\mu_0$) increases, and the electromagnetic turbulent transport would degrade the confinement or β [14]. In some cases, electromagnetic turbulence can be driven to be unstable by the temperature gradient or impurity density gradient in finite-β plasmas [15–17]. In the presence of impurity ions, theoretical work has studied the underlying electrostatic turbulence or the isotope effect on the turbulence [18–23]. Specifically, an impurity mode can be driven by the impurity density gradient in the case of the outwardly peaked impurity profile [18]. One possible physical mechanism is that the Landau damping from the main ions can be weakened by impurity ions [23]. However, there have been fewer experimental and theoretical works which have investigated the effect of the impurity ions on electromagnetic turbulence. This Letter reports the observation of an edge peaked impurity profile in *H*-mode plasmas, self-regulated by an electromagnetic turbulence excited with double impurity critical gradients. It reveals the possible mechanism for an active control of pedestal dynamics and ELMs via pedestal turbulence.

Experimental results presented in this Letter are based on the phenomenon of cyclic transitions between the intermediate confinement phase (*I phase*) and the *H* mode under the constant auxiliary heating power in the HL-2A

Tokamak, whose major and minor radius are $R = 1.65$ and $a = 0.4$ m, respectively. In these experiments, the electron density and temperature profiles were measured by the microwave X-mode reflectometry and the ECE radiometer, respectively. The electromagnetic turbulence was detected by Mirnov coils. The electrostatic turbulence was measured by the microwave reflectometry near the pedestal top ($r \simeq 35$ cm). The reflectometry measurement is localized close to the reflection layer and sensitive to the turbulence with radial wave number $k_r < 2.5$ cm^{-1} according to the numerical simulation [24]. The plasma radiation was obtained by a 2D bolometer array. The impurity line emission was given by a vacuum ultraviolet spectrometer. Figure 1(a) shows the traces of plasma current of 160 kA, toroidal magnetic field of 1.3 T and NBI heating power of 1.1 MW. The time evolution of the divertor D_α signal [Fig. 1(b)] shows a distinctive feature in the H mode and I phase. In the H-mode phase, the plasma has a very low recycling rate shown by the extremely low intensity of the D_α signal, and the plasma stored energy W_E and the line-averaged electron density $n_{\rm el}$ increased during this phase as seen in Fig. 1(c). The carbon impurity ion C v (2271 Å, $1s2s\,^3S$-$1s2p\,^3P$) is increased as shown in Fig. 1(d). Owing to the low ionization energy ($E_i = 392$ eV), it is located around the pedestal region. Meanwhile, the averaged impurity density estimated by the ratio of total radiation power to line-averaged electron density ($P_{\rm rad}/n_{\rm el}$) is also increased, indicating the formation of a radiation layer localized at the plasma edge as shown in Fig. 1(f). The duration of the stationary phase of the H mode is $5 \sim 10$ ms. In the I phase, the D_α signal displays quasi-periodic perturbations caused by limit cycle oscillations

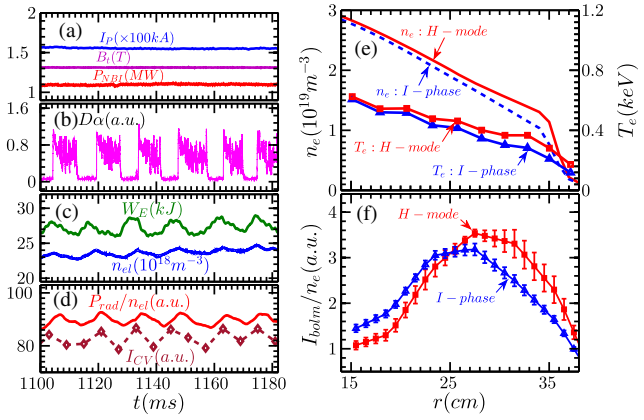

FIG. 1. Time evolution of the main parameters in a typical discharge with cyclic transitions: (a) plasma current I_p, toroidal magnetic field B_t and NBI heating power $P_{\rm NBI}$, (b) divertor D_α signal, (c) inner stored energy W_E and line-averaged electron density $n_{\rm el}$, (d) the ratio of total radiation power to line-averaged electron density ($P_{\rm rad}/n_{\rm el}$) and intensity of carbon impurity ion C v 2271 Å. Profiles of (e) electron density and temperature, and (f) indication of the impurity density $I_{\rm bolm}/n_e$ in the I phase and H mode.

(LCOs) that have been intensively studied [25–27]. In contrast, due to the considerable particle loss induced by electrostatic turbulence modulated by LCOs, the confinement of plasma particles and impurities is degraded during the I phase. Then the plasma transits into the H mode from the $10 \sim 20$ ms I phase due to the edge pressure gradient exceeding the threshold [28]. Figure 1(f) displays the radial profile of $I_{\rm bolm}/n_e$, here $I_{\rm bolm}$ is the emissivity reconstructed from bolometer array that is mainly contributed by intrinsic impurity. Generally, this ratio can be considered as the effective impurity density [29,30]. For simplification, the symbol n_z denotes $I_{\rm bolm}/n_e$ in the following. Figure 1(f) shows an outwardly peaked profile in the edge, contrary to the inwardly peaked profiles of electron temperature and density as shown in Fig. 1(e), indicating that the impurities accumulated close to the pedestal top. The edge impurity accumulation was also observed in C-Mod with the same diagnostic [30]. Figure 1(e) illustrates the edge electron density and temperature profiles in the H mode and I phase, showing enhanced plasma confinement of the H mode compared to the I phase.

Behaviors of impurity density during cyclic I-H transitions are shown in Fig. 2. During the H-mode phase, the impurities are gradually accumulated in the edge region ($r = 25$–35 cm) as seen in Fig. 2(b). The impurity accumulation is ended by the triggering of an ELM represented by a large spike in D_α signal [Fig. 2(a)]. Meanwhile, the maximum absolute value of the normalized impurity gradient $R/L_{n_z} = R\nabla n_z/n_z$ in the positive and negative gradient region increases as shown in Figs. 2(c) and 2(d), respectively. Then the pedestal impurity gradient has undergone a drastic drop due to the ELM flushing effect on the impurity as shown in Fig. 2(d). While the R/L_{n_z} in the positive gradient region [Fig. 2(c)] decreases slowly owing to the inward propagation of the ELM flushing effect.

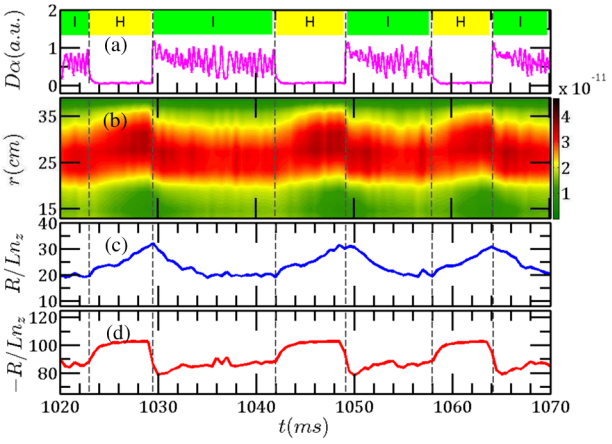

FIG. 2. (a) Divertor D_α signal and the indications of the I phase and H mode. (b) Spatiotemporal evolution of n_z, maximum n_z gradient in the positive (c) and negative (d) gradient region.

The dynamic process of the impurities is repetitive when the plasma transits repeatedly between the I phase and H mode as shown in Fig. 2. It should be noted that the $|R/L_{n_z}|$ in the negative gradient region [Fig. 2(d)] swiftly increases by a period of 1–2 ms and then saturates during the ELM-free phase of the H mode. It suggests that there might be a mechanism which can limit the further increase of the impurity gradient in the quasistationary plasma edge, where no ELMs or large scale coherent modes appear.

Figures 3(b) and 3(c) show the spectrogram of magnetic and density fluctuations measured by Mirnov coil and reflectometry, respectively. In the H-mode phase, following the impurity accumulation in the edge region, it has been observed that the electromagnetic turbulence explodes and is then ended with the onset of the ELM as shown in Fig. 3(b). As expected, the spectrogram in Fig. 3(c) shows that the electrostatic turbulence is considerably reduced in the H-mode phase compared with that in the I phase. However, residual electrostatic fluctuation can be observed during the occurrence of the electromagnetic turbulence. The coherency between $\tilde{B}_\theta$ and $\tilde{n}_e$ is calculated by $\gamma(\tilde{B}_\theta, \tilde{n}_e) = |P_{\tilde{B}_\theta,\tilde{n}_e}|^2/(P_{\tilde{B}_\theta,\tilde{B}_\theta} P_{\tilde{n}_e,\tilde{n}_e})$, where $P_{\tilde{B}_\theta,\tilde{n}_e}$ is the cross-power spectrum, $P_{\tilde{B}_\theta,\tilde{B}_\theta}$ and $P_{\tilde{n}_e,\tilde{n}_e}$ are the auto-power spectra. Figure 3(d) shows the comparison of the coherency between the H mode and I phase. It shows that the coherency $\gamma(\tilde{B}_\theta, \tilde{n}_e)$ in the frequency range of 50–100 kHz is noticeably higher in the H-mode case than that in the I phase. By integrating the $\gamma(\tilde{B}_\theta, \tilde{n}_e)$ over the frequency range of 50–100 kHz, the time evolution of the integrated coherency $\int \gamma df$ is obtained and shown in Fig. 3(e). The integrated coherency has a higher level in the H-mode period than that in the I phase. It means that the turbulence detected by the microwave reflectometry is the potential component of the electromagnetic turbulence. This indicates that the electromagnetic turbulence is located around the pedestal top. The trace of its magnetic fluctuations in H-mode periods is shown in Fig. 3(f). Figure 3(g) is the trace of its intensity, showing the exponential growth and then saturation of the turbulence accompanying with the peaking of the edge n_z profile.

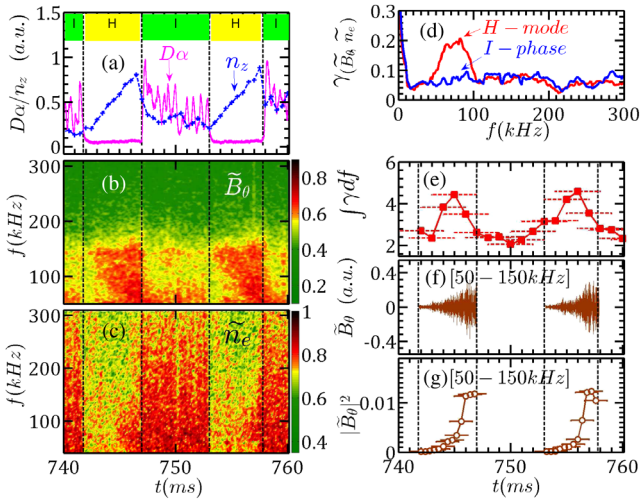

FIG. 3. (a) Divertor D_α signal, edge n_z and the indications of I (I phase) and H (H mode), spectrogram of magnetic (b) and density (c) fluctuations, (d) coherency spectra between magnetic and density fluctuations in I phase and H-mode phase, (e) time evolution of integrated coherency over the frequency domain of 50–100 kHz, (f) filtered magnetic fluctuations and (g) the intensity evaluated by the square of the root- mean-square (RMS) envelope in two H-mode phases.

Figure 4(a) displays the contour plot of the electromagnetic turbulence spectrogram during the H-mode phase. At the beginning, the turbulence is generated around 140 kHz as a coherent mode. Immediately, the turbulence frequency spectrum is broaden, and the central frequency shifts down. The toroidal rotation velocity of the plasma is higher in the H-mode phase than that in the I phase. Thus, the Doppler shift induced by the plasma rotation is excluded for the observed frequency downshift. Figure 4(b) plots the frequency spectrum width of the turbulence as a function of the turbulence intensity, showing linear and saturation regimes. For $|\tilde{B}_\theta|^2 < 0.004$, the width Δf is proportional to the intensity $|\tilde{B}_\theta|^2$, while the width Δf is saturated for $|\tilde{B}_\theta|^2 \geq 0.004$. This indicates that the nonlinear effect becomes dominant at a very moderate level of turbulence. Figure 4(c) is the autobispectrum $B^2(f_1, f_2) = \langle |\hat{X}(f_1)\hat{X}(f_2)\hat{X}^*(f_1 + f_2)|^2 \rangle$, where $\hat{X}(f)$ is the Fourier transform of magnetic fluctuations and $\hat{X}^*(f)$ is the complex conjugate [31,32]. The $B^2(f_1, f_2)$ is an indicator for the strength of nonlinear coupling of three waves at f_1, f_2, and $f_1 + f_2$. The angular brackets represents the ensemble average. The summed

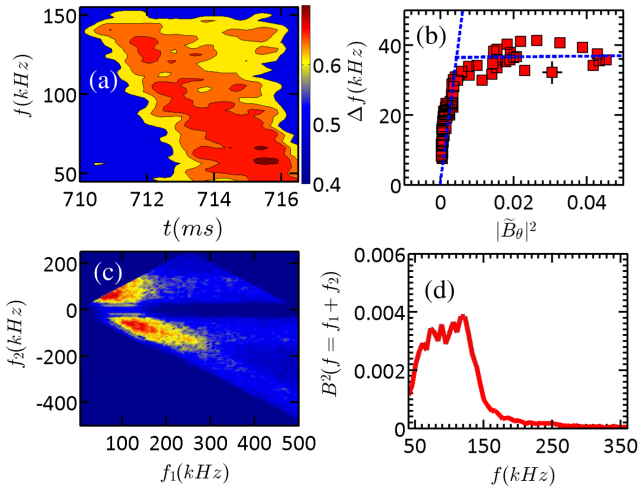

FIG. 4. (a) Contour plot of the electromagnetic turbulence spectrogram during the H-mode phase, (b) correlation between the frequency spectrum width of the turbulence and the turbulence intensity, (c) autobispectrum of magnetic fluctuations during the H-mode phase and (d) its summed bispectrum.

bispectrum shown in Fig. 4(d) is defined as $B^2(f) = [1/N(f)]\sum_{f=f_1+f_2} B^2(f_1, f_2)$, where the sums are taken over the area in the $f_1 - f_2$ domain satisfied with the matching condition $f = f_1 + f_2$ and N is the number of the satisfied elements. The autobispectrum and summed bispectrum show that the turbulence in the frequency range of 50–150 kHz has high spectrum intensity. The result reveals that the electromagnetic turbulence exhibits strong nonlinear coupling by three-wave interaction. This frequency shift with generation of a broadband spectrum could be originated from the inverse energy cascade of the turbulence from small to large scale due to the strong nonlinear mode interaction [33].

Previous analysis indicates that the excitation of the electromagnetic turbulence might be related to the edge impurity gradient. The result in Fig. 5(a) shows the measured intensity of the electromagnetic turbulence $|\tilde{B}_\theta|^2$ as a function of R/L_{n_z} in positive and negative gradient regions. In the positive gradient region, when the R/L_{n_z} exceeds $R/L_{n_z} \simeq 25$, the turbulence intensity $|\tilde{B}_\theta|^2$ increases steeply, meaning there is a critical gradient of the impurity for the excitation of the electromagnetic turbulence. Similarly, a critical gradient of $-R/L_{n_z} \simeq 102$ is also observed in the negative gradient region. The critical value of $|R/L_{n_z}|$ in the positive gradient region is much lower than that in the negative region. Theoretical work has predicted that the electrostatic impurity mode can be excited in the presence of impurity ions with an outwardly peaked density profile [18]. However, there were fewer theoretical works that have addressed the electromagnetic model with impurity ions. In this work, the effects of the carbon impurity ions on electromagnetic turbulence have been studied with a gyrokinetic code HD7, which is used to solve the electromagnetic integral eigenmode equations for the study of drift instability [16,17]. It includes a complete gyrokinetic description for both the main and impurity ion species. In the simulations, the carbon impurity ion (C^{4+}), which was the main impurity in this experiment, was considered. The corresponding charge concentration $f_c = Zn_z/n_e$ is assumed to be $f_c = 0.3$, where Z is the charge number. The magnetic shear is $s = 2$ and the toroidal beta of electron β is 0.6%. Figure 5(b) displays the simulated linear growth rate normalized by electron diamagnetic drift frequency ω_{*_e} as a function of R/L_{n_z}. It also shows double critical gradients in R/L_{n_z}. For the excitation mechanism, the mode is driven by the impurity density gradient in the positive R/L_{n_z} region. In the negative R/L_{n_z} region, the mode is driven by both impurity and electron density gradients. Detailed theoretical analysis can be found in Ref. [34]. Figure 5 shows that the strong asymmetry of two critical gradients from simulation is consistent with the experimental observation. It suggests that the observed electromagnetic turbulence could belong to a kind of drift instability which exhibits an electromagnetic feature. The magnetic fluctuations could affect the electron confinement on magnetic flux surfaces. In addition, it is expected to affect the impurity transport, since it is driven by the impurity density gradient.

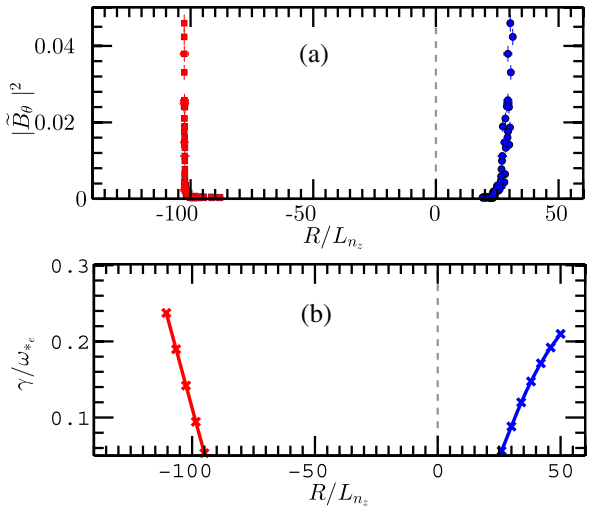

FIG. 5. (a) Experimental result: the relation between the intensity of electromagnetic turbulence and the normalized impurity density gradient, (b) electromagnetic simulation by the HD7 code: the normalized linear growth rate of electromagnetic turbulence versus the normalized impurity density gradient.

In the experiment, the edge peaked impurity profile is self-regulated by the impurity gradient driven turbulence as described in the following. After the transition from the I phase into the H-mode phase, the electrostatic turbulence is considerably reduced and the impurity ions are accumulated at the edge due to the formation of the edge transport barrier. An electromagnetic turbulence is excited and exponentially increases when the impurity gradients exceed the critical values. The ELM-free phase is ended with the onset of the ELM burst. After the ELM, the impurity is immediately exhausted, and the plasma transits into the I phase, with the generation of strong electrostatic turbulence modulated by LCOs. With the gradually increasing pedestal pressure gradient during the I phase, the plasma returns to the H-mode regime. Thus, cyclic transitions between the I phase and the H mode are spontaneously controlled by impurity gradient driven electromagnetic turbulence.

In summary, a broadband (frequency of 50–150 kHz) electromagnetic turbulence has been observed in the HL-2A H-mode plasmas. The generation of the broadband spectrum and the frequency down-shift of the turbulence could be due to the inverse energy cascade mechanism. The turbulence excitation is strongly correlated to the accumulation of impurity at the edge. Double impurity critical gradients have been observed for the excitation of the turbulence. The critical value of $|R/L_{n_z}|$ in the positive gradient region is much lower than that in the negative region. This strong asymmetry in the critical gradient has

been quantitatively confirmed by theoretical simulation. The simulation indicates that the impurity density gradient is the driving source of the electromagnetic turbulence in the positive R/L_{n_z} region, while the excitation of the turbulence in the negative R/L_{n_z} region is determined by both impurity and electron density gradients. HL-2A experimental results revealed that the edge peaked impurity profile is self-regulated by the impurity driven turbulence with double critical gradients. This result suggests that the quasistationary edge-localized impurity profile offers the possibility to actively control the pedestal dynamics and ELMs via pedestal turbulence, which helps to protect plasma facing components.

The authors would like to thank the HL-2A team for the support of the experiments, gratefully acknowledge M. Kikuchi for stimulating discussions and helpful suggestions. This work is partially supported within the framework of the cooperation between the French Commissariat à l'Energie Atomique et aux Energies Alternatives (CEA) and the China National Nuclear Corporation (CNNC). It is partially supported by Natural Science Foundation of China under Grants No. 10990213, No. 11305053, No. 11475057, No. 11275062, and No. 11375057, and partially supported by Chinese National Fusion Project for ITER under Grants No. 2013 GB107000 and No. 2014 GB108000.

*Corresponding author.
zhongwl@swip.ac.cn

[1] F. Wagner, G. Fussmann, T. Grave *et al.*, Phys. Rev. Lett. **53**, 1453 (1984).
[2] F. Wagner, Plasma Phys. Controlled Fusion **49**, B1 (2007).
[3] H. Zohm, Plasma Phys. Controlled Fusion **38**, 105 (1996).
[4] J. W. Connor, Plasma Phys. Controlled Fusion **40**, 531 (1998).
[5] A. Kallenbach, M. Bernert, R. Dux *et al.*, Plasma Phys. Controlled Fusion **55**, 124041 (2013).
[6] A. Kallenbach, M. Bernert, T. Eich, J. C. Fuchs, L. Giannone, A. Herrmann, J. Schweinzer, and W. Treutterer, Nucl. Fusion **52**, 122003 (2012).
[7] S. Jachmich, G. Maddison, M. N. A. Beurskens *et al.*, Plasma Phys. Controlled Fusion **44**, 1879 (2002).
[8] G. P. Maddison, C. Giroud, B. Alper *et al.*, Nucl. Fusion **54**, 073016 (2014).
[9] C. Giroud, G. P. Maddison, S. Jachmich *et al.*, Nucl. Fusion **53**, 113025 (2013).
[10] G. T. Hoang, C. Bourdelle, X. Garbet, G. Giruzzi, T. Aniel, M. Ottaviani, W. Horton, P. Zhu, and R. V. Budny, Phys. Rev. Lett. **87**, 125001 (2001).
[11] P. Mantica, D. Strintzi, T. Tala *et al.*, Phys. Rev. Lett. **102**, 175002 (2009).
[12] D. Villegas, R. Guirlet, C. Bourdelle, G. T. Hoang, X. Garbet, and R. Sabot, Phys. Rev. Lett. **105**, 035002 (2010).
[13] W. L. Zhong, X. L. Zou, C. Bourdelle, S. D. Song, J. F. Artaud, T. Aniel, and X. R. Duan, Phys. Rev. Lett. **111**, 265001 (2013).
[14] M. Kikuchi and M. Azumi, Rev. Mod. Phys. **84**, 1807 (2012).
[15] F. Zonca, L. Chen, R. A. Santoro, and J. Q. Dong, Plasma Phys. Controlled Fusion **40**, 2009 (1998).
[16] J. Q. Dong, L. Chen, and F. Zonca, Nucl. Fusion **39**, 1041 (1999).
[17] G. M. Lu, Y. Shen, T. Xie, L. Qi, Z. He, H. He, and S. Cui, Phys. Plasmas **20**, 102505 (2013).
[18] B. Coppi, H. P. Furth, M. N. Rosenbluth, and R. Z. Sagdeev, Phys. Rev. Lett. **17**, 377 (1966).
[19] K. T. Tsang, Nucl. Fusion **17**, 261 (1977).
[20] N. Mattor, Phys. Fluids B **3**, 2153 (1991).
[21] S. Migliuolo, Nucl. Fusion **32**, 1331 (1992).
[22] J. Q. Dong and W. Horton, Phys. Plasmas **2**, 3412 (1995).
[23] S. F. Liu, C. L. Zhang, W. Kong, S. C. Guo, J. Q. Dong, L. M. Liu, Q. Liu, and Z. Y. Liu, Europhys. Lett. **97**, 55004 (2012).
[24] X. L. Zou, L. Laurent, and J. M. Rax, Plasma Phys. Controlled Fusion **33**, 903 (1991).
[25] R. J. Colchin, M. J. Schaffer, B. A. Carreras *et al.*, Phys. Rev. Lett. **88**, 255002 (2002).
[26] R. J. Colchin, B. A. Carreras, R. Maingi *et al.*, Nucl. Fusion **42**, 1134 (2002).
[27] G. R. Tynan, M. Xu, P. H. Diamond *et al.*, Nucl. Fusion **53**, 073053 (2013).
[28] J. Cheng, J. Q. Dong, K. Itoh *et al.*, Phys. Rev. Lett. **110**, 265002 (2013).
[29] M. Greenwald, R. Boivin, P. Bonoli *et al.*, Phys. Plasmas **6**, 1943 (1999).
[30] A. Diallo, J. W. Hughes, S.-G. Baek *et al.*, Nucl. Fusion **55**, 053003 (2015).
[31] Y. C. Kim and E. J. Powers, IEEE Trans. Plasma Sci. **7**, 120 (1979).
[32] D. Gresillon and M. S. Mohamed-Benkadda, Phys. Fluids **31**, 1904 (1988).
[33] H. Xia and M. G. Shats, Phys. Rev. Lett. **91**, 155001 (2003).
[34] Y. Shen *et al.* (to be published).